ORIGINAL PAPERS

A kinetic study of the photolysis of sulfamethoxazole with special emphasis on the photoisomer

Wolf-Ulrich Palm[1] · Nicola Schmidt[1] · Marcel Stahn[2] · Stefan Grimme[2]

Abstract

The previously not studied photochemical degradation of sulfamethoxazole (SMX) to the isomer of SMX (ISO) was measured via a polychromatic (Xe) and a monochromatic (Hg) light source and accompanied by quantum chemical DFT calculations. In addition to the $pK_a = 7.0 \pm 0.1$ of ISO, tautomer-dependent properties such as the K_{OW} were measured and theoretically confirmed by DFT. The kinetics in solutions below and above the $pK_a = 5.6$ of SMX were studied for the available and quantifiable products SMX, ISO, 3-amino-5-methylisoxazole (AMI), 2-amino-5-methyloxazole (AMO), and sulfanilic acid (SUA). The quantum yields of the neutral (Φ_N) and anionic Φ_A) forms of SMX ($\Phi_A = 0.03 \pm 0.001$, $\Phi_N = 0.15 \pm 0.01$) and ISO ($\Phi_A = 0.05 \pm 0.01$ and $\Phi_N = 0.06 \pm 0.02$) were found to be wavelength-independent. In a competitive reaction to the formation of ISO from SMX, the degradation product TP271 is formed. Various proposed structures for TP271 described in the literature have been studied quantum mechanically and can be excluded for thermodynamic reasons. In real samples in a northern German surface water in summer 2021 mean concentrations of SMX were found in the range of 120 ng/L. In agreement with the pH-dependent yields, concentrations of ISO were low in the range of 8 ng/L.

Graphical abstract
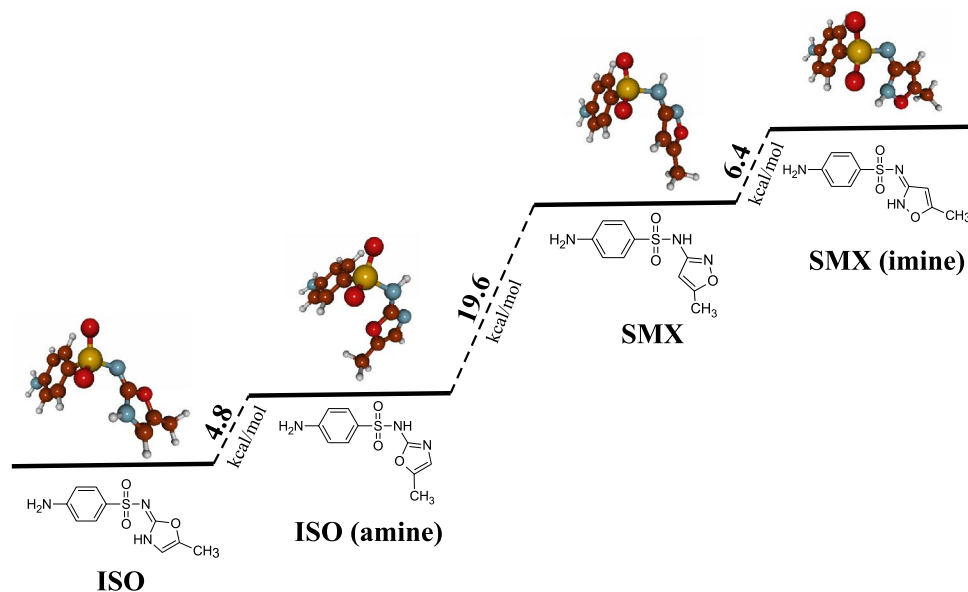
Keywords Kinetics · Quantum yields · Quantum chemistry · DFT · Surface water

✉ Wolf-Ulrich Palm
 palm@uni.leuphana.de

Extended author information available on the last page of the article

1 Introduction

Sulfamethoxazole (SMX) is a common human and veterinary antibiotic. Due to its great importance, at least as a member of the sulfonamide family, production and usage, as well as concentrations and environmental sources and sinks of SMX, have been presented and summarized in various reviews [1–6]. Highly variable concentrations of SMX ($LOQ < c/ng\ L^{-1} < 16,700$) are found in rivers worldwide [7], with a reported mean concentration of $\bar{c} = 76$ ng L^{-1} ($c_{median} = 14$ ng L^{-1}) [8] and a range of $\bar{c} < 10 - 60$ ng L^{-1} [9] in European Rivers. Due to its frequent usage in medication, concentrations of SMX are discussed as a marker for the origin of wastewater (i.e., WWTP-effluent) [10].

As early as 1994, direct photolysis was first described as a potential degradation pathway of SMX in aqueous solutions by Zhou and Moore in a landmark paper [11]. However, the obvious potential of SMX as a chemical actinometer for natural sunlight [12] was not further explored. In a wealth of work in the following years, in addition to direct photolysis (e.g., [13–36]), the degradation of SMX via bimolecular processes initiated by light together with, e.g., hydrogen peroxide [31, 37, 38], ozone [19, 39–42], chlorine [34], chlorine dioxide [43], a combination of ozone and hydrogen peroxide [20, 44] or by UV/persulfate [33] was published. A general overview of the removal of SMX from aqueous solutions is given in [45], an overview of the many transformation products reported in the literature in [46].

In the early papers by Zhou and Moore [11, 12], significant key points of direct photolysis of SMX have already been addressed. For the first time the importance of the second dissociation constant of SMX ($pK_{a2} = 5.6$) in explaining the pH-dependent UV spectra, rate constants, and quantum yields was discussed. Furthermore, the separation of main products by preparative HPLC, characterization by, e.g., NMR-spectroscopy and the degradation by sun-light of SMX depending on the season was presented. The cleavage of the bond connecting the sulfonamide and isoxazole part and addition of water was recognized as the source of the main products sulfanilic acid (SUA) and 3-amino-5-methylisoxazole (AMI). In addition, the well-known photochemical isomerization of the isoxazole part [47] of SMX via an azirine intermediate [48, 49] was used to explain the formation of the corresponding oxazole-derivative, hereafter referred to as ISO:
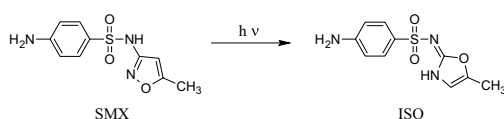
As with the 3-aminoisoxazoles [50], the energetically preferred tautomer in SMX is present as an amine. In contrast, ISO is preferentially present as an imine [11]. Although the formation of ISO has been found to be one of the major photoproducts of SMX and has been reported in numerous subsequent publications [21, 33, 37, 51–54], the correct imine structure is often ignored.

In addition to the rearrangement of SMX, the hydrolysis of the azirine intermediate as a competitive reaction provided an explanation of an assumed ring-opening product with molar mass $M = 271$ g mol^{-1} (TP271) [11]. However, besides the adoption of the original structure [21, 54, 55], and although TP271 was characterized by, e.g., NMR-spectroscopy, in later investigations, different structures for TP271 were suggested [23, 33, 52, 54, 56, 57].

Missing experiments of the photolysis of ISO and contradictory statements on structures and products were the starting point of the investigations presented here. The study includes

- the analysis of SMX and ISO and UV-spectra and properties of ISO,
- a kinetic analysis of the pH-dependent photolysis of SMX and ISO including the main products,
- an overview of available pH-dependent quantum yields of SMX including recommended values and a comparison with corresponding quantum yields of ISO,
- an assessment of the many reported structures of TP271 by DFT methods,
- concentrations found for SMX and ISO in surface waters from a River in North-Germany.

2 Experimental

2.1 Analytical procedures

Sulfamethoxazole (SMX) and all other compounds were analysed by LC–MSMS (HPLC 1200, Agilent, with dual pump, autosampler, column oven and mass spectrometer 6430, Agilent). Conditions HPLC: column Agilent Poroshell 120 SB-C18 4.6 × 30 mm; particle size 2.7 µm; eluent: A = methanol, B = 0.1% formic acid, $0'-3'$: 5% A, $3'-6'$: gradient to 80% A, $6'-6.1'$: gradient to 5% A, $6.1'-9'$: 5% A; $T = 25$ °C; injection volume = 5 µL; needle wash; flow rate = 1 mL/min. Conditions mass spectroscopy: ESI-head, positive mode, source parameters: $T = 350$ °C, gas flow = 10 L/min, p(nebulizer) = 35 psi, capillary voltage = 4000 V. LC–MSMS parameter and exemplified chromatograms are summarized in the Supplementary Information (SI, Table S1 and Figure S1). Quantification was performed with external calibration solutions relative to internal standards (IS) sulfamethoxazole-D4 (SMX-D4), sulfanilic acid-D4 (SUA-D4)

and aniline-d5 (ANI-D5) in the range of $c = 0 − 1000$ μg/L for all compounds using linear calibration functions. Therefore, usually in 100 μL-inserts $V = 45$ μL of a sample is combined with $V = 5$ μL of the IS-mixture ($c_0 = 1000$ μg/L).

Sum formulas of isomers and transformation products were checked by high-resolution mass spectrometry (HRMS, Thermo Scientific, Dionex UltiMate UHPLC system with LTQ Orbitrap-XL).

UV-spectra (double-beam spectrometer Lambda 45 with pre monochromator, Perkin Elmer) were measured with a resolution of 2 nm in 1 nm steps at $d = 1$ cm in quartz cuvettes at ambient temperature with the solvent as reference. The wavelength accuracy has been checked by a holmium filter to be better than $\Delta\lambda = \pm 1$ nm.

UV-spectra ($d = 1$ cm) were obtained with concentrations in the range of $5 − 20$ mg L^{-1} versus the corresponding solvent. For the measurement of the pK_a-value of ISO ($c_0 = 10$ mg/L), mixtures of phosphoric acid (0.1 M), potassium dihydrogenphosphate (0.1 M) and sodium hydroxide (0.1 M) were used to prepare pH-values $3.5 \le$ pH ≤ 11, determined by a pH-electrode SenTix 940-3 and SenTix Mic-D (WTW, Weinheim, Germany) after calibration with standard buffer solutions at pH $= 4$ and 7. The pK_a-value was evaluated using the Henderson–Hasselbalch equation as mean value of absorbances at 7 pH-values from 18 wavelengths between 207 and 281 nm.

For the measurements of $\log(K_D)$ (distribution coefficient octanol/buffer) suitable prepared and with octanol saturated buffer solutions and n-octanol, saturated with the corresponding buffer solution, were used. Mixtures of n-octanol and buffer ($V = 0.5–2$ mL) of ISO with concentrations of $c_0 = 10−400$ μg L^{-1} were shaken (Heidolph Reax 2) at $T = 20 \pm 2$ °C for 2 h in Eppendorf safe-lock tubes (2 mL). After centrifugation (centrifuge miniSpin, Eppendorf) for 5 min at 10,000 rpm the n-octanol phase was directly analysed by LC–MSMS.

2.2 Photolysis in the laboratory, actinometry and quantum yields

The setup for photolysis experiments is described elsewhere [58]. In brief, photolysis experiments were performed with a photolysis apparatus on an optical bench (Amko, Tornesch,Germany) with a Xe lamp XBO 1000 (Osram, Germany). The electrical power of the light source was always set to 500 W ($\pm 2\%$). Light was focused by mirrors through an optical glass-filter with known absorbance into a stoppered quartz cuvette ($d = 1$ cm) with the corresponding solution ($V_{start} = 3135$ μL) equipped with a stirring bar in a cuvette holder with magnetic stirrer. The distance between light source and cuvette was 70 cm. The Xe lamp

and mirrors were cooled by tap water, cooling of the cuvette ($T = 293 \pm 1$ K) was accomplished by a thermostat (Type Petite Fleur, Huber, Germany). Experiments always started with an equilibrium period to stabilize the light source and temperature in the stirred solution (5–10 min). Within the equilibrium period, the light beam was shut off with a shutter behind the optical filter. After taking three dark samples within 2 min ($V = 45$ μL) for irradiation time $t = 0$ s, the shutter was opened and the solution was irradiated. Usually 10 samples were removed ($V = 45$ μL) after a given irradiation time (accuracy of about 1 s) within a maximum irradiation time of $t = 500$ min. Always air saturated solutions were used from solutions stirred at least 60 min before start in the dark at room temperature. Oxygen concentrations were determined by an oxygen digital IDS-sensor FDO (WTW, Weinheim, Germany).

A second, identical optical bench was used for irradiation by a (not cooled) monochromatic mercury-light source (UVP PenRay Lamp, $\lambda = 254$ nm, Analytik Jena US) in a distance of 56 mm to the entrance window of the thermostated cuvette. To remove the 185 nm line of the PenRay lamp a home-made optical filter prepared from microscope slides (quartz-glass, $d = 3$ mm) was used.

Relative light intensities were obtained with a SpectraWiz Spectrometer (Black-Comet C-25 Spectrometer, StellarNet Inc., USA). Actinometric measurements for both polychromatic and monochromatic light sources using iron(III)oxalate are described in detail elsewhere [59].

Details in the calculation of quantum yields for the experimental setups discussed above are available in [58, 59]. For the low concentrations used in this study quantum yields Φ (dimensionless [60]) were calculated from Eq. (1) in steps of $\Delta\lambda = 1$ nm. Parameters in Eq. (1) are the rate constant k_{exp} (in s^{-1}) from the photolysis of the compound, the spectral photon irradiance on amount basis I_λ (in mol s^{-1} cm^{-2} nm^{-1}) from actinometry, the molar decadic absorption coefficient ϵ_λ (in L mol^{-1} cm^{-1}) from UV-spectroscopy and the conversion factor 2303. From this definition the quantum yield is, therefore, the fraction of the experimental rate constant, k_{exp}, and the theoretical maximal rate const, $k_{\Phi=1}$, with a quantum yield for a primary process of $\Phi = 1$

$$\Phi = \frac{k_{exp}}{2303 \sum_{\lambda(start)}^{\lambda(end)} I_\lambda \epsilon_\lambda \ \Delta\lambda} = \frac{k_{exp}}{k_{\Phi=1}} \qquad (1)$$

In Eq. (1) $\lambda(\text{start})$ is defined by the onset of the light spectrum and $\lambda(\text{end})$ by the end of the UV-spectrum.

Based on the available data for different light sources (vide infra), it can be expected for SMX and at least assumed for ISO that the quantum yield is wavelength independent.

2.3 Analysis in river samples

Concentrations of SMX and ISO from 5 sampling campaigns between February 2020 and September 2021 (winter and summer) were used. Therefore, 80 samples obtained in a small river in the northern part of Germany (River Wietze, length about 45 km) with two main inflows and with in sum 3 WWTP as exclusive sources of SMX were quantified after SPE-enrichment and analysis by LC–MSMS as described in [61]. A map of the sampling points and detailed concentrations are summarized in the SI (Table S4 and S5 and Figure S9).

2.4 Compounds and solutions

Formic acid (98–100%), phosphoric acid (85%), sodium hydroxide (> 99%) and potassium dihydrogenphosphate (100%) were purchased from Merck and VWR (Germany) and solvents (acetonitrile, methanol) were purchased from VWR in the highest available quality (> 99.7%) and were used as received. Potassium trioxalatoferrate(III) trihydrate (Alfa Aesar, 99%) was recrystallized from water. Ultra pure water with a specific resistance of 18.2 MΩ cm was produced from a water-purification system (OmniaTap UV, Stakpure, Germany).

Sulfamethoxazole (abbreviated SMX, supplier Ehrenstorfer, purity 99.0%), 4-amino-*N*-(5-methyl-2-oxazolyl)benzenesulfonamide (ISO, TLC Pharmaceutical Std., 99.6%), sulfanilic acid (SUA, TCI, > 99 %), 3-amino-5-methylisoxazole (AMI, TCI, > 97%), 2-amino-5-methyloxazole (AMO, Vlada Chem, > 95%) and aniline (ANI, Aldrich, 99.5%) were used as received. Sulfamethoxazole-D4 (SMX-D4, HPC Standards, 99.5%), sulfanilic acid-D4 (SUA-D4, TRC, 98.0%) and aniline-D5 (ANI-D5, CIL, ≥ 98%) were used as internal standards in the LC–MSMS analysis.

Stock solutions of SMX, ISO, SUA, AMI, AMO and ANI in acetonitrile with concentrations of c(stock) = 1000 mg L^{-1} each and SMX-D4, SUA-D4 and ANI-D5 in acetonitrile with concentrations of c(stock) = 100 mg L^{-1} (for ANI-D5 1000 mg L^{-1}) each were stored in the dark at $T = -25$ °C and were used in the preparation of dilutions and for calibration solutions. Diluted working solutions (c_0 = 1000 μg L^{-1}) for photolysis experiments were always freshly prepared from stock solutions and the corresponding solvent (e.g., dist. water, buffer).

2.5 Description of the kinetic model

This study focused especially on the direct photolysis of SMX and ISO in buffered solutions with start concentrations below $c \leq 2\,\mu M$ ($\leq 500\,\mu g\,L^{-1}$) and without additives to prevent for instance the formation of OH-radicals. For the photon flux of the polychromatic Xe-light source and within the time range of $t \leq 500$ minutes loss reactions of AMI, AMO und SUA were negligible and set to zero. However, as discussed below, in photolysis reactions starting with ISO, a loss of AMO in basic solutions at pH = 8.5 was found. In a global model, equations summarized in the SI (Chapter S4.2 and S4.3) were used in parallel in a non-linear fit [62] for both cases starting with SMX or ISO. These cases include all compounds and for the fit relative concentrations of c(SMX), c(ISO), c(AMI), c(AMO), c(SUA) and c(ISO2) (see below for the discussion of the isomer ISO2) were used by division of the absolute concentrations by the start concentration c_0(SMX) or c_0(ISO), respectively. All equations are based on 1st-order kinetics and are derived from the description of fundamental consecutive and parallel reactions [63]. The reaction scheme and the assignment of the rate constants for the case c_0(SMX) > 0 and c_0(ISO) = 0 is shown in Fig. 5. The rate constant $k = k_1 + k_2 + k_{SUA} + k_S$ describes the loss of SMX, the rate constant $k' = k_3 + k_{ISO2} + k_I$ the loss of ISO. The rate constant k_1 describes the formation of ISO, k_2 the formation of AMI (and the corresponding equimolar formation of SUA), k_3 the formation of AMO (and the equimolar formation of SUA), k_S unknown loss reactions for SMX and k_I corresponding unknown loss reactions for ISO. These rate constants are involved for both basic and acidic conditions starting with SMX. Starting from ISO, all rate constants directly related to SMX are zero and the scheme, therefore, simplifies drastically (see SI Chapter S4.2 and S4.3).

In the case of c_0(SMX) > 0 in addition three special rate constants were included into the kinetic scheme. For basic conditions it was found that c(SUA) > c(AMI) + c(AMO) and it was necessary to include an additional formation reaction for SUA, represented by k_{SUA}. From the accuracy of the experimental data it was not possible to distinguish formation reactions of SUA directly from SMX or ISO or via (unknown) intermediate products. For simplicity reasons an additional formation of SUA from SMX was used comparable to the formation of AMI but with unknown products from the original isoxazole ring in SMX. For both acidic and basic conditions very low, and therefore, highly uncertain concentrations of a further isomer of SMX (ISO2) were found in the photolysis of SMX and ISO. However, for basic conditions even LC–MSMS areas (and estimated concentrations) were too low to be quantifiable. This unknown isomer is also formed from ISO without delay, typical for a direct formation and not as a product of a subsequent reaction (see the Sect. 3). Therefore, a direct formation from ISO is assumed with the rate constant k_{ISO2} and the loss reaction k'_{ISO2}.

In the case of c_0(ISO) > 0 besides k_{SUA} in addition a rate constant for the loss of AMO (k_{AMO}) at high pH was necessary.

2.6 Quantum chemical calculations

Using density-functional theory (DFT), it is possible to predict Gibbs free energies of molecules starting from their geometry as input purely theoretically.

At finite temperatures, the description of a molecule by a single geometric (and corresponding electronic) structure can be unrealistic. With increasing molecular flexibility, a large number of conformers may exists within a very narrow energy window. All significantly populated conformers at a given temperature form a conformer ensemble (CRE) that determines the properties of the system. The population of conformer i is given by the Boltzmann distribution:

$$p_i = \frac{e^{\frac{-G_i}{kT}}}{\sum_i^{\text{conf.}} e^{\frac{-G_i}{kT}}}, \qquad (2)$$

where p_i is the probability of a given conformer to be populated, G_i is the Gibbs free energy of conformer i, k is the Boltzmann constant and T the temperature of the system. Due to the flexibility of the investigated molecules, it was necessary to extensively screen their conformational space as described in [64]. CREs were created with the general force field GFN-FF [65] and irrelevant conformers were sorted out using the semiempirical GFN2-xTB [66] method using the CREST [67] program. The resulting CRE was then re-ranked on a higher DFT level of theory using the r2SCAN-3c [68] composite method. All these steps were paired with an implicit solvation model [69–71] for water, to take solvation effects into account.

The Gibbs free energies of the amine and imine tautomers of SMX and ISO, as well as of the TP271 derivatives were finally calculated as a Boltzmann weighted average over the energies of the relevant conformers as

$$\overline{G} = \sum_i^{\text{conf.}} p_i G_i. \qquad (3)$$

Dipole moments for AMO, AMI, ISO and SMX were calculated accordingly by averaging over all relevant conformers.

The pKa value of AMO was calculated also at the r2SCAN-3c level from the CREs of the corresponding acid and base as described in [72]. The accuracy of this approach is estimated to be about ± 0.5 pK_a units for a wide range of molecules.

3 Results and discussion

3.1 Overview of compounds considered

LC–MSMS parameters and exemplary chromatograms are summarized in the SI (Table S1 and Figure S1, Figure S2) with detection limits in the range of DL = 2–7 nM. Only substances available as reference compounds and known to be products in the direct photolysis of SMX (and assumed of ISO) were used in the quantitative kinetic analysis. Therefore, ISO, 3-amino-5-methylisoxazole (AMI) and sulfanilic acid (SUA) were considered in the photolysis of SMX and the corresponding oxazole-derivative 2-amino-5-methyloxazole (AMO) and again SUA in the photolysis of ISO.

In addition to a large number of products formed by direct and indirect photolysis of SMX and detected by HRMS in assumed low concentrations, e.g., [21, 43, 56, 73], only a few products are available as reference compounds. These compounds include human metabolites, such as nitroso, nitro and hydroxylated derivatives of SMX [21, 74], also discussed in biotic degradation reactions [75], formed in, e.g., ozonolysis or indirect photolysis reactions [37, 42, 76–78] and explicitly avoided in this work and not considered in detail. In agreement with other studies [14, 33, 55, 57, 79], aniline was not found in any of the samples from experiments performed here. However, these results are in contradiction to experiments, where aniline is formed in the photolysis of SMX [11, 21, 42, 43]. It is interesting to note that the seldom reported and in this study not considered product (5-methyl-1,2-oxazol-3-yl)sulfamic acid in the photolysis of SMX [21, 42, 43] was always found together with aniline. Furthermore, unlike other sulfonamides, elimination of SO$_2$ does not play a role for SMX [80].

Besides SMX and ISO another isomer of SMX (ISO2) was found in the photolysis of SMX and ISO. The sum formula of this third isomer was obtained via HRMS. The mass-to-charge ratio for protonated SMX and isomers is m/z (theo, C$_{10}$H$_{12}$N$_3$O$_3$S$^+$) = 254.05939, the experimental value for all isomers was identical to m/z ([SMX+H]$^+$ = [ISO+H]$^+$ = [ISO2+H]$^+$) = 254.0602 ($\Delta m/z$ = 3 ppm). The isomer ISO2 is formed from ISO and was, therefore, found in both photolysis reactions starting with SMX or ISO. The retention time of ISO2 (t_r = 6.16 min, see also SI, Figure S2) was the highest retention time of all compounds analysed (SI, Figure S1) and ISO2 is assumed to be the amine tautomer of ISO (vide infra). Very low concentrations of ISO2, estimated from the response of ISO, were found in the range of 0.1–0.5 mol% of ISO.

The last compound considered in more detail is the transformation product TP271, found at a retention time of 3.1 min. The sum formula of TP271 was obtained by comparison

Table 1 Properties of SMX and ISO

Property	SMX	Note	ISO	Note
$\epsilon_{max}(\lambda)/M^{-1}\,cm^{-1}$ at pH 3.5	16,980 (268)	A	19,080 (264)	A
			14,100 (243)	
$\epsilon_{max}(\lambda)/M^{-1}\,cm^{-1}$ at pH 8.8	17,210 (256)	A	17,450 (252)	A
Solubility (pH)/g L^{-1}	0.391 (5.41)	B	> 40 (H_2O)	I
	6.112 (7.17)	B		
	0.372 (H_2O)	C		
$pK_{a2} \pm \sigma$	5.6 ± 0.04	D	7.0 ± 0.1	A
$\log(K_D)$ (pH)	− 0.76 (7.6)	E	⌐0.87 ± 0.6 (9)	A
	0.83 (4)	F	− 0.38 ± 0.08 (7)	A
	0.71 (5.6)	F	− 0.33 ± 0.09 (5)	A
	− 0.4 (7.5)	F		
	− 0.91 (8.5)	F		
$\log(K_{OW})$	0.89	G		
	0.72 (amine)	H	0.91 (amine)	H
	− 0.81 (imine)	H	− 1.15 (imine)	H

Maxima (ϵ_{max}) in the UV-spectra at wavelength λ, pH-dependent solubilities in water, dissociation constant pK_a between neutral and anionic structure, pH-dependent distribution constants $\log(K_D)$ and partition constant $\log(K_{OW})$ between octanol/water. A: (20 ± 2) °C this work B: 25 °C [86] C: 25 °C [87] D: (23 ± 1) °C [81] E: [88] F: 25 °C [89] G: pH=6.4 [90] H: this work, from DFT calculations as described in Ref.[91] for the imine and amine tautomer I: estimation at 25 °C for the most favorable imine-tautomer [92]

of the theoretical mass-to-charge ratio for protonated TP271 (m/z (theo, $C_{10}H_{14}N_3O_4S^+$) = 272.06995) with the experimental value of the only peak in the chromatogram of m/z ([TP271+H]$^+$) = 272.0689 ($\Delta m/z = -4$ ppm). TP271 was characterized in [11] and the formation was explained as a byproduct in a hydrolysis reaction of the azirine-derivative leading to ISO (see Fig. 7). A theoretical study was performed (Sect. 3.5) to assess the thermodynamic stability using standard Gibbs free energies calculated for numerous products reported in the literature (see Sect. 1).

3.2 Properties of SMX and ISO and UV-spectra

Some basic properties of SMX and ISO are summarized in Table 1. Sulfonamides possess two dissociation equilibria [14, 81–83]. The equilibrium between cationic and neutral SMX is characterized by $pK_{a1} = 1.6$ [14], the equilibrium between neutral and anionic SMX by $pK_{a2} = 5.6$ [81]. The pK_{a2} of ISO was determined in this study to be $pK_{a2} = 7.0 \pm 0.1$ (see UV-spectra in the SI, Figure S6). The protonation at the amine group of 4-amino-benzenesulfonamide is $pK_a = 1.78$ [84] and comparable to the first pK_{a1} of known sulfonylamides [14, 81]. Hence, for ISO a pK_{a1} comparable to known sulfonylamides can be assumed and indeed no further change in the UV-spectra of ISO was

found between $3.5 < pH < 6$. As additional information the $pK_a = 3.28$ (at $T = 20$ °C) of SUA [85], the $pK_a = 0.47$ of AMI [50] and the theoretically determined $pK_a = 6.60$ of AMO should be mentioned.

As for AMO and AMI, theoretical calculations indicated a prefered population of the amine tautomer for SMX ($\Delta G^{-\ominus-}_{imine \rightarrow amine} = -6.4$ kcal mol^{-1}). On the other hand, for ISO a preferred population of the imine tautomer ($\Delta G^{-\ominus-}_{amine \rightarrow imine} = -4.8$ kcal mol^{-1}) was found (see Fig. 1).

These results are in agreement with qualitative experimental findings for AMI [50] and SMX and ISO [11]. Calculated dipole moments for the imine tautomers of AMO, AMI, ISO and SMX were found to be higher (but for SMX nearly comparable) than the corresponding amine-tautomers (see SI, Table S2). The imine tautomers discussed in this study can thus be assumed to be at least slightly more polar than the amine tautomers.

Corresponding differences could also be found for the octanol/water distribution constants K_{OW} and K_D by DFT calculations (see Table 1). For the imine tautomers of SMX and ISO $\log(K_{OW})$ are much lower and negative compared to the amine tautomers. Accordingly experimental values of $\log(K_D)$ between pH = 5–9 for ISO are always negative with $\log(K_{OW}) = -1.15$ calculated by DFT. The reverse is true for SMX with positive $\log(K_D)$ for pH < pK_{a2} [89] and $\log(K_{OW}) = 0.89$ [90].

UV-spectra of SUA [54], AMI [50, 54] and SMX [20, 21, 26, 52, 54] with molar decadic absorption coefficients at different pH-values are available in the literature in agreement with values presented in this study (SI, Figure S5 and Figure S7). In addition the up to now not published UV-spectra for AMO are also included in the SI (Figure S7).

The UV-spectra of ISO below and above pK_{a2} are shown in Fig. 2, qualitatively discussed for pH < pK_{a2} in the literature [11]. The UV spectrum of ISO (and completely analogous for SMX) in acetonitrile is virtually identical to the UV spectrum of the neutral compound in the aqueous phase. The shoulder (at 243 nm) in the UV-spectrum of ISO at pH=3.3 is an indicator of the imine structure [11].

3.3 Photolysis of SMX and ISO

No other isomer (i.e., no ISO) was found in stock solutions of SMX, and a very low impurity of < 0.1 mol% of SMX was found in stock solutions of ISO (SI, Figure S2). The kinetic curves obtained from two measurements each with the polychromatic Xe-light source for pH = 3.7 and pH=8.8 are shown in Figs. 3 and 4 (a typical spectrum of the polychromatic Xe-light source is shown in Fig. 2).

The kinetic scheme used is shown in Fig. 5, the rate constants obtained for all reactions involved from the overall fit of the reactions in Fig. 5 are summarized in the SI (Table S3 and Chapter S4.2 and S4.3) and for the calculation of the

Fig. 1 DFT calculated standard Gibbs free reaction enthalpies $\Delta_R G^{-\ominus-}$ of the amine and imine tautomers of SMX and ISO relative to the most stable ISO isomer
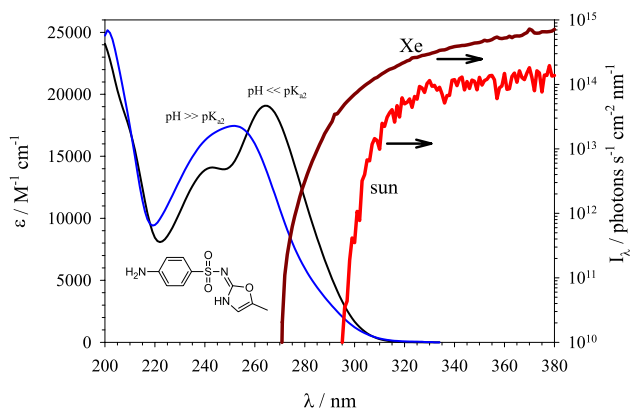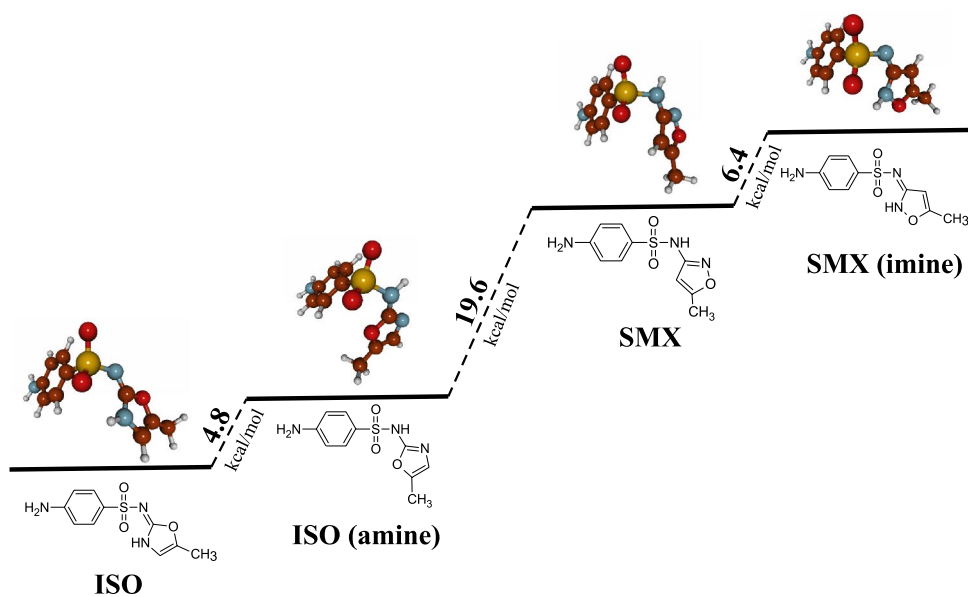

Fig. 2 Molar decadic absorption coefficients (left scale) of ISO in buffered solutions at pH = 3.5 (pH $\ll$ pK_{a2}) and at pH = 8.5 (pH $\gg$ pK_{a2}). For comparison a typical spectrum of the polychromatic Xe-light source used in this study and a sun-spectrum (calculated with the STAR model [93]) for the 21.6.2021 at 52.3 °N, 10.4 °E, 11 UTC (right scale) is shown

Fig. 3 Normalized concentrations and kinetics of compounds quantified in the photolysis of SMX with a Xe-light source at pH = 3.7, $T = 20\,°C$ and $c_0(SMX) \pm \sigma = (1.92 \pm 0.05)\,\mu M$. Lines are from a global model with all compounds involved, summarized in Fig. 5, Table 2 and the SI (Table S3). Note the different scalings of the ordinates

quantum yields of SMX and ISO in Table 2. The different yields (in percent) given in Fig. 5 of the compounds formed in acidic and basic solution were calculated by the fraction of the corresponding formation-rate constant and the loss-rate constant of SMX or ISO.

In acidic aqueous solution, AMI and SUA are formed from SMX in equimolar concentration. However, in basic solution a lower concentration of AMI than for SUA is obtained with a consequently additional formation for SUA (8 mol%) with unknown reaction of the original isoxazole ring. For simplicity, it was assumed that this additional pathway forms SUA directly and not via unknown intermediates. The SUA fraction of 20 mol% formed in basic
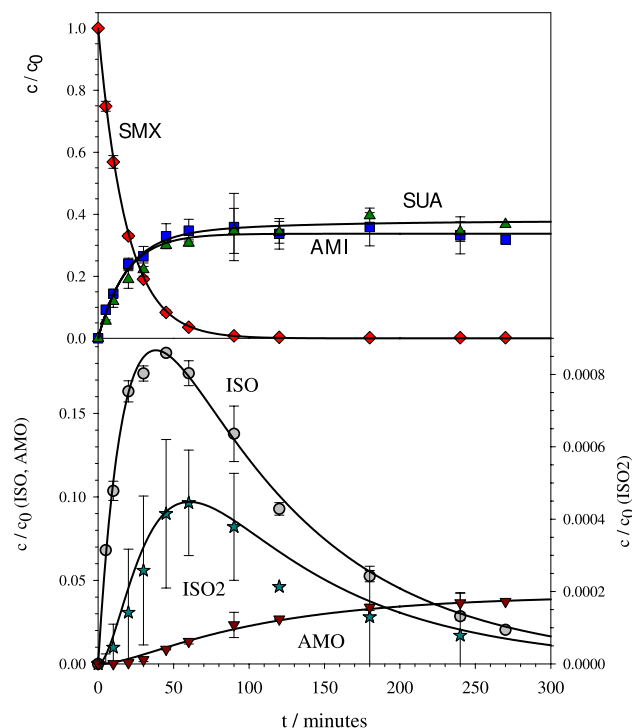
solution and about 30 mol% in acidic solution is in agreement with values in [14] (35 mol% at pH=2) and [21] (20 mol%, but pH not specified). In [73] the direct photolysis
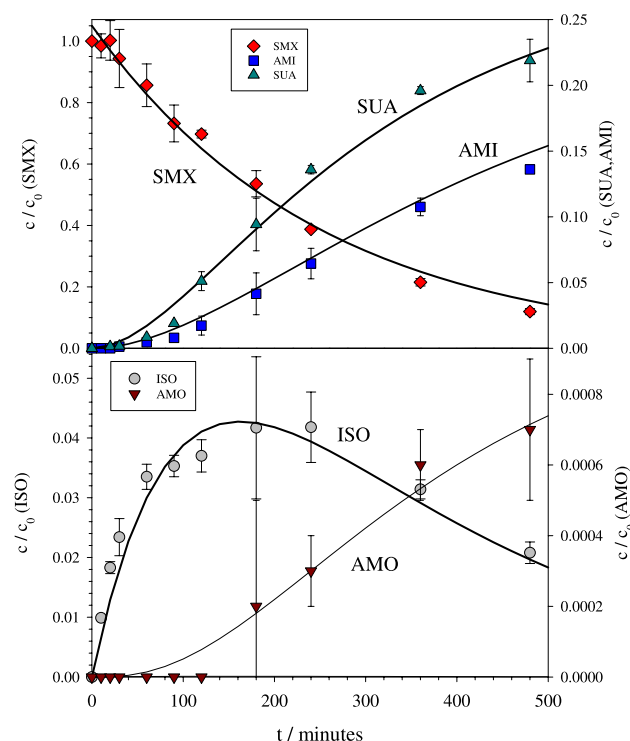
Fig. 4 Normalized concentrations and kinetics of compounds quantified in the photolysis of SMX with a Xe-light source at pH = 8.8, $T = 20\ °C$ and $c_0(SMX) \pm \sigma = (2.10 \pm 0.04)\ \mu M$. Lines are from a global model with all compounds involved, summarized in Fig. 5, Table 2 and the SI (Table S3). Note the different scalings of the ordinates

of a high mass concentration of $c(SMX) = 100\ mg\ L^{-1}$ in unbuffered water leads to comparable mass concentrations of AMI and SUA of about 10 mg L^{-1}, i.e., in a molar ratio of AMI : SUA ≈ 2 : 1. Only a very low yield of 2% for AMI (but a higher yield of 11% of (5-methyl-1,2-oxazol-3-yl)sulfamic acid and 5% of aniline) was reported in [21]. In our measurements AMI was found to be stable in all solutions at different pH-values and for different light sources.

Due to the $pK_a = 3.28$, the formation of SUA has a significant impact in unbuffered water on the development of the direct photolysis of SMX and ISO, especially if high start concentrations are used. An example is shown in the SI (Figure S8) for the development of the pH-value in the photolysis of ISO with the Hg-light source. Even for moderately concentrated start concentrations of $c(ISO) = 13\ \mu M$ (= 3.3 mg/L) a change of almost $\Delta pH = 0.8$ covering the important pH = 7 (i.e., pK_{a2} of ISO) was found.

The formation of ISO in the photolysis of SMX, first reported in [11, 12], was also stated in [21, 33, 52, 54, 55], in [51] the time development of ISO was monitored by LC–MSMS.

In no case a photochemical back reaction of ISO to SMX was observed in this study. The yield of ISO of 28 mol% found in acidic solution is comparable to the estimated yield of 30 mol% given in [11]. In [15] the analysis of the reaction solution by LC–MSMS indicated that ISO was not formed through a OH-mediated reaction. Besides photolysis, other formation reactions of ISO in the dark are known. ISO is reported to be formed by microbially initiated one-electron reductive cleavage of the isoxazole N–O bond in SMX via the azirine intermediate [94] or in an electro-Fenton process [95]. AMO was assumed in addition or besides AMI [14], and assumed as a possible product (only at pH = 9) from ISO [37]. As for all other reaction pathways, the formation of AMO is pH dependent. Concentrations of AMO found in this study were low and rate constants of the formation and loss of AMO (see SI, Table S3) are uncertain. AMO was stable in acidic solutions using the polychromatic and the monochromatic light source, but was photolysed in basic solution. Concentrations of AMO in photolysis experiments of SMX with start concentrations of 2 μM were too low to be used in the evaluation of rate constants (see Fig. 4). From an independent performed photolysis of AMO with the Xe-light source at pH = 8.5 and the photolysis starting from ISO at pH=8.8 (see SI, Table S3) a highly uncertain rate constant of $k_{AMO} \pm \sigma = (0.007 \pm 0.004)\ min^{-1}$ (considering different photon irradiances by about a factor of 2) with $\Phi_{AMO} \pm \sigma = (0.1 \pm 0.06)$ was obtained.

Besides SMX and ISO a third isomer ISO2 was detected and concentrations were estimated from the response of SMX and ISO. Concentrations at pH = 3.7 are already low (about 0.5 mol% with respect to and starting from SMX and 2 mol% with respect to and starting from ISO) and were too low at pH=8.8 to be quantified. The kinetics of the formation of ISO2 starting from SMX and ISO is shown in the SI, Figure S3. As expected ISO2 is directly formed starting from ISO and in a consecutive reaction via ISO starting from SMX. This kinetic behaviour supports, therefore, the assumption that ISO2 is formed from ISO. Furthermore, and as already stated above, ISO2 degrades in a dark reaction at $T = 20\ °C$ in acidic solution as the only compound investigated with a lifetime of $\tau = 109$ h (see SI, Figure S4). These experimental facts and, in addition, the highest retention time of all isomers suggest that ISO2 may be the relatively non-polar amine tautomer of ISO (see Fig. 1).

3.4 Quantum yields

To evaluate the quantum yields of ISO, quantum yields of SMX were also measured for comparison. All experiments were performed at $T = 20\ °C$ and were, furthermore, carried out with the polychromatic Xe light source and the monochromatic Hg lamp. An extraordinary number of quantum yields for SMX have been reported in the literature, some

Fig. 5 Results of the photolysis of SMX with a Xe-light source at pH = 8.8 (see Fig. 4, equation arrows in blue) and at pH = 3.6 (see Fig. 3, equation arrows in red) at T = 20 °C. Percentages are fractions of the different reaction channels in basic (in blue) and in acidic (in red) solution
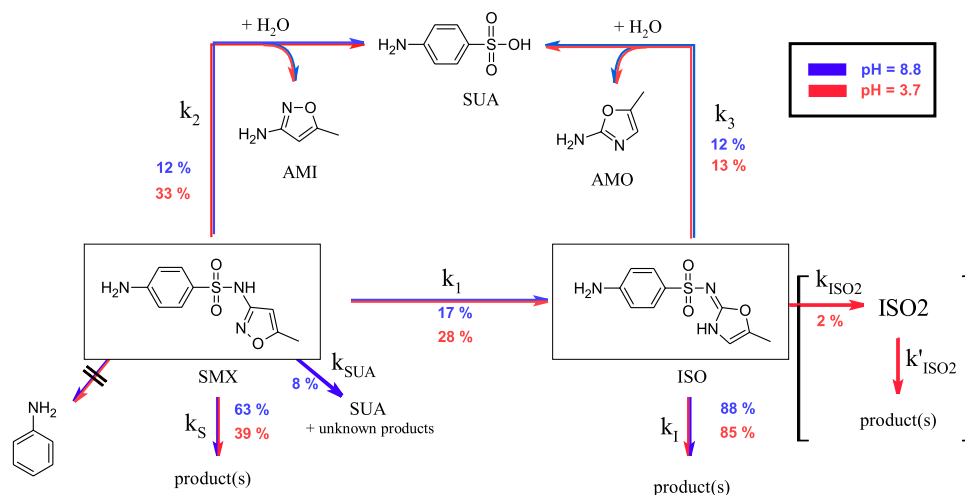
of which are contradictory. The unusually large database prompted us to calculate recommended quantum yields below (Φ_N) and above (Φ_A) the pK_{a2} from the available data. However, contrary to the large number of quantum yields of SMX in aqueous solutions, surprisingly, no quantum yields of SMX in organic solvents are known. In addition to prospective measurements in various organic solvents (data not discussed here), the quantum yields of SMX and ISO in acetonitrile were determined.

Quantum yields of SMX and ISO in aqueous solutions with necessary parameters such as rate constants and photon irradiances are summarized in Table 2. With the given errors, quantum yields independent of the light source were obtained for all pH values and mean values were used.

The mean quantum yield of SMX determined in this study for both light sources (polychromatic Xe-lamp and monochromatic Hg-light source) at pH = 3.7 is $\Phi_N = 0.15 \pm 0.01$, at pH = 8.6 $\Phi_A = 0.03 \pm 0.001$. As discussed above, a pH = 3.7 is assumed to be above pK_{a1} of ISO. The

corresponding quantum yield of ISO determined in this study for both light sources at pH = 3.7 is $\Phi_N = 0.06 \pm 0.02$, at pH = 8.6 $\Phi_A = 0.05 \pm 0.01$.

Quantum yields in acetonitrile from two independent measurements starting from SMX and ISO are $\Phi = 0.12$ (SMX) and $\Phi = 0.09$ (ISO) and are thus comparable to the corresponding quantum yields Φ_N. However, in contrast to the measurements in the acidic environment, a very low yield of 1% of ISO but a high yield of 55% of AMI is found in acetonitrile.

With the dissociation fraction α and the quantum yields of the neutral species, Φ_N, and the anionic species, Φ_A, the apparent quantum yield is $\Phi = \Phi_N \cdot (1 - \alpha) + \Phi_A \cdot \alpha$. Substitution of the dissociation fraction α from the Henderson–Hasselbalch equation leads to

$$\Phi = \Phi_N + \frac{\Phi_A - \Phi_N}{10^{pK_{a2}-pH} + 1} \tag{4}$$

Table 2 Quantum yields Φ and corresponding rate constants k (in min^{-1}) of sulfamethoxazole (SMX) and the isomer of SMX (ISO) from 11 kinetic runs in buffered aqueous solutions at 20 °C

	SMX				ISO			
pH	3.7	3.7	8.5	8.8	3.7	3.7	8.5	8.6
Light source	Hg	Xe	Hg	Xe	Hg	Xe	Xe	Xe
N	11	2×12	11	2×12	12	2×12	12	12
c_0	1.8	1.9	1.7	2.1	1.3	2.0	2.2	2.0
I	0.76	173	0.76	173	0.76	218	218	218
k(SMX)	0.200	0.054	0.057	0.0039	–	–	–	–
Φ(SMX)	0.155	0.140	0.028	0.030	–	–	–	–
k(ISO)	0.130	0.010	0.122	0.008	0.146	0.013	0.018	0.017
Φ(ISO)	0.073	0.038	0.061	0.034	0.082	0.039	0.061	0.058

Errors ($\pm\sigma$) in k are in the range of 5–10%, errors in Φ in the range of 10–20%. pH = pH of the solution. Light source = Hg: monochromatic light source λ = 254 nm; Xe: polychromatic xenon-light source $\lambda > 280$ nm. N = number of irradiation times. c_0/μM = start concentration of SMX and ISO, respectively. I/nmol s^{-1} cm^{-2} = photon irradiance in the wavelength region 280–560 nm (Xe) or 254 nm (Hg) from actinometry
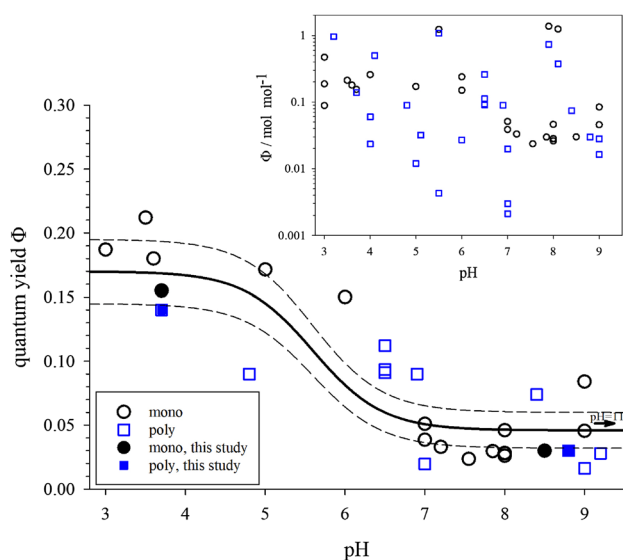
Fig. 6 Plot of $N = 30$ recommended pH-dependent quantum yields Φ of SMX versus pH ($3 \leq$ pH ≤ 9). All quantum yields found in the literature are shown in the insert excluding values around pK_{a1}, at undefined pH-values (i.e., pure water) and below $\Phi < 0.001$. Circles = quantum yields using monochromatic light sources, squares = quantum yields using polychromatic light sources, filled symbols = this work. The solid line is the result from a fit of Eq. (4), the dotted lines are values for $\Phi \pm 2\sigma$. Any error bars given are not shown for clarity

In sum $N = 69$ pH-dependent quantum yields of SMX were found in the literature (details in an Excel-sheet in the SI). Quantum yields of SMX at or below pK_{a1} with $\Phi \approx 0$ [14, 23, 36] and quantum yields in water [15–17, 25, 29] with undefined pH were excluded. From the remaining ($N = 58$) quantum yields published in [11–15, 17–36] recommended values ($N = 30$) were used from [11, 12, 14, 18,

20, 21, 24, 26, 27, 31–36] in a non-linear fit from Eq. (4) to obtain Φ_A and Φ_N (see Fig. 6).

Quantum yields of SMX using values from monochromatic light sources only ($N = 19$) are $\Phi_N \pm 2\sigma = 0.19 \pm 0.03$ and $\Phi_A \pm 2\sigma = 0.040 \pm 0.014$, from polychromatic light sources only ($N = 11$) are $\Phi_N \pm 2\sigma = 0.13 \pm 0.05$ and $\Phi_A \pm 2\sigma = 0.057 \pm 0.028$ and for all values ($N = 30$) $\Phi_N \pm 2\sigma = 0.17 \pm 0.03$ and $\Phi_A \pm 2\sigma = 0.046 \pm 0.014$ (fit shown in Fig. 6). The quantum yields for the different light sources, identical within measurement errors, imply that both Φ_N and Φ_A for SMX and ISO do not depend on wavelength. Accordingly, SMX as well as ISO are examples of compounds that satisfy the Kasha–Vavilov rule [96, 97].

3.5 Formation of TP271

As already discussed in the Introduction, closely related to the formation of ISO from SMX is a side reaction of the intermediate azirine derivative shown in Fig. 7.

The formation of the transformation product TP271, described and characterized in [11], was explained from the hydrolysis of the azirine derivative. Homolytic cleavage at bond A (see Fig. 7) leads to ISO, cleavage at bond B provides the back reaction to SMX. A heterolytic cleavage and reaction with water at bonds A and B yields four potential products. TP271 [11] and the never described isomer TP271d are reached via pathway A, while TP271b, described in [94], as well as TP271e, reported in [23], are obtained via pathway B.

For deriving the structure of TP271, NMR spectra, MS spectra and chemical methods were used [11], for all other alternative structures shown in Table 3 no evidence other than MS fragments or even only MRM transitions were used. To assess the importance of isomers TP271a–TP271h

Fig. 7 Possible products from the azirine-derivative formed as intermediate after photolysis of SMX. Cleavage of the bonds A and B in the azirine derivative and subsequent hydrolysis or rearrangement leads to 6 different compounds (including the back-reaction to SMX itself). The product TP271d was never mentioned in the literature, for differences in ΔG see Table 3
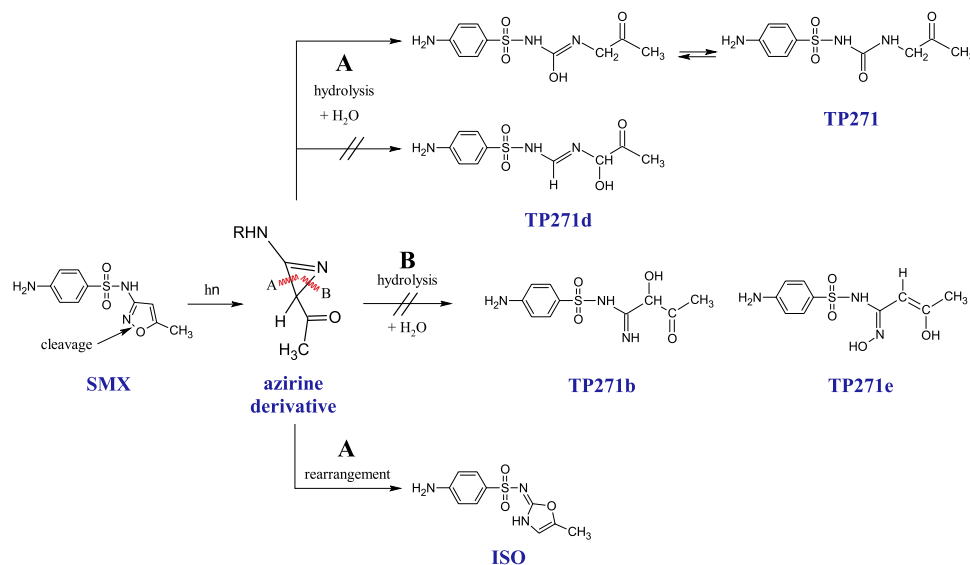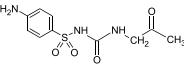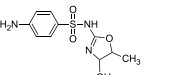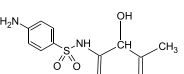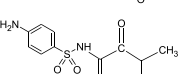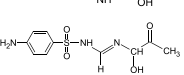
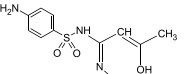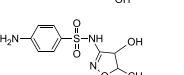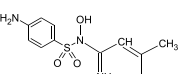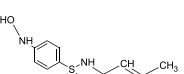**Table 3** Transformation products with a molar mass of $M = 271$ g mol^{-1} reported in the literature and their $\Delta_R G^{-\ominus-}$-values (in kcal mol^{-1}) calculated in this study by DFT relative to TP271

Name	Structure	$\Delta_R G^{-\ominus-}$ kcal mol^{-1}	Lit.
TP271		0	[11, 21, 54, 55]
TP271a		18.7	[33]
TP271b		21.9	[94]
TP271c		25.9	[23]
TP271d		26.2	See Fig. 7
TP271e		51.7	[56]
TP271f		56.8	[52, 54, 57]
TP271g		57.3	[56]
TP271h		57.8	[56]

reported in the literature in comparison with TP271 $\Delta_R G^{-\ominus-}$ was calculated relative to TP271. $\Delta_R G^{-\ominus-}$ thus corresponds to the reaction of the isomers TP271a–TP271h to TP271, respectively. The calculated data summarized in Table 3 show, that the thermodynamically most stable isomer is TP271. Accordingly, the quantum mechanical calculations provide very strong arguments that the given structures for TP271a–TP271h as transformation products in the direct photolysis of SMX are not correct. Thus, if a transformation product with the molecular formula $C_{10}H_{13}N_3O_4S$ is found in the direct photolysis of SMX, it is very likely to be TP271.

3.6 Environmental concentrations in river water

SMX and ISO were also analysed as part of campaigns in 2020/2021 in the Wietze, a small river in Northern Germany (latitude 52.6 °N). Details on sampling and preparation of the aqueous samples for analysis by LC–MSMS are compiled in [61]. The sampling area, location of the sample sites, and details of the concentrations obtained are summarized in the SI (Chapter S5).

Survey measurements between February 2020 and September 2021 provided mean daily concentrations for SMX in the river water ranging from $c = 43 - 337$ ng L^{-1}, strongly dependent on the volume flow of the Wietze River and thus also on the season. As expected variations in concentrations of SMX in the effluent of the largest WWTP were much lower with values of $c = 319 - 748$ ng L^{-1}. In none of the analysed 80 samples ISO could be found above the limit of quantification ($LOQ = 2$ ng L^{-1}).

On June 28, 2021 ten monitoring sites in a special "summer campaign" were sampled in a section of the Wietze River without tributaries over a distance of 9 km. In these measurements with a pH = 7.7 mean concentrations were $c(\text{SMX}) \pm \sigma = (121 \pm 17)$ ng L^{-1} and $c(\text{ISO}) \pm \sigma = (8 \pm 2)$ ng L^{-1}. The concentrations of ISO are consistent compared to the concentrations of SMX due to the 17% yield in the basic environment (see Fig. 5) and the higher degradation rate constant of ISO relative to SMX (see Table 2).

Even for the special "summer campaign" for none of the compounds a decrease (SMX) or increase (ISO) of the concentration in the watercourse of the Wietze could be proven. A rough estimation of the minimum half-life of SMX (and ISO) is possible from the uncertainty of concentrations found. A minimum half-life for SMX in surface water is obtained for $t = 5$ h (calculated from the distance of 9 km and a flow rate of $v = 0.5$ m s^{-1}) and an assumed maximum decrease in concentration of 20%. However, this half-life, valid for the time of measurement, must be corrected and increases by about a factor of 2–3, since all measurements were made over noon with maximum solar radiation and the day–night cycle must be considered. Taking all these factors into account the minimum half-life of SMX in the Wietze River for a summer day is $t_{1/2} \gg 45$ h.

For comparison qualitative information about the abiotic degradation of SMX with a light source simulating sunlight [22, 56, 98] and calculated and measured half-lives for sunlight are available. Reported half-lives of SMX in the literature are highly variable. Even for similar time periods and latitudes, values are given that differ by more than a factor of 10. Thus, pH plays a significant role in addition to the quantum yield itself (for calculated values). SMX, and thus presumably ISO, is predominantly degraded even in natural waters via direct photolysis [14, 98]. In addition, the concentrations of nitrate and DOC (e.g., also via an internal filter effect [13]) as well as morphological parameters such as water depths influence the half-lives in model scenarios or in laboratory measurements.

Thus, for the latitude 47 °N in acidic solution half-lives with $t_{1/2} = 10.4$ and 44 h (summer/winter) [21] or for the latitude 50 °N in acidic solution $t_{1/2} = 58$ h for winter [14] were given. Much higher half-lives at pH=7 of $t_{1/2} = 300$ h and 750 h (summer/winter) for latitude 22.3 °N

are calculated in [27] via the SMART model and in [30] at pH = 7 for the summer period of $t_{1/2} = 96 - 2160$ h using the Apex model for variable water parameters.

Furthermore, half-lives measured in sunlight (May–June) for Minneapolis (USA, latitude 45 °N) in buffer solutions were given as $t_{1/2} = 5$ h (pH = 5.3) and $t_{1/2} = 35$ h (pH = 6.9) [14] and for Sydney (Australia, latitude 33.55 °S) in acidic solution as $t_{1/2} = 1$ and 9.6 h (summer/winter) [12].

4 Conclusions

The predominant presence of the tautomeric amine structure in SMX and the imine structure in ISO defines the properties of both compounds and should always be correctly reproduced. The direct photolysis of SMX and of ISO below and above the respective pK_a value proceeds at different rates with different yields of the analysed compounds. The yield for ISO from photolysis of SMX above pK_{a2} is only about half as large (17 mol%) compared to the yield in the acidic range (28 mol%). Using the products SUA, AMI and ISO, the mass balance found for the photolysis of SMX in the acidic range (pH < pK_{a2} is roughly 60%, and only 40% in the basic range. In the corresponding photolysis of ISO using the products SUA and AMO, the mass balance is extremely poor in all pH ranges with < 15%.

Concentrations of SMX and ISO were further measured in natural samples from a surface water body in the Wietze river, a typical river in the North German Plain. A degradation of SMX or an increase of ISO could not be found in the Wietze river even in a summer campaign in 2021 for a, however, small flow distance of 9 km. In agreement with the measured quantum yield of ISO from SMX for pH > pK_{a2} of $\Phi = 0.05$, the mean concentrations of ISO are low at $c(ISO) = 8$ ng L^{-1} compared with the mean concentrations for SMX of $c(SMX) = 120$ ng L^{-1}. From the analytical uncertainties half-lives of SMX and ISO in the range of days for the summer months for latitudes in the northern part of Germany were estimated. Assuming a degradation of both compounds by direct photolysis and the reduction of available sun-light intensities in winter half-lives of both compounds in a surface water in winter are assumed to be in the range of weeks.

The found quantum yields of SMX and of ISO are independent of the wavelength within the experimental errors. However, various measurements reported in the literature on the quantum yields of SMX are doubtful or not comparable with other values due to insufficient specification of, e.g., the pH value. Thus, out of 69 quantum yields found, only roughly half were used to calculate the quantum yield of the anionic and the neutral form of SMX.

Besides the formation of ISO from SMX, a competing reaction is the formation of the transformation product TP271. Many alternative structures, often insufficiently characterised, have been reported in the literature (products TP271a-TP271h). A quantum mechanical calculation of the free enthalpies of these products yields the result that all alternative structures are significantly higher in energy and must, therefore, be regarded as insignificant.

Declarations

References

1. Kümmerer, K. (2009). Antibiotics in the aquatic environment—A review—Part I. *Chemosphere, 75,* 417–434. https://doi.org/10.1016/j.chemosphere.2008.11.086.

2. Kümmerer, K. (2009). Antibiotics in the aquatic environment—A review—Part II. *Chemosphere, 75,* 435–441. https://doi.org/10.1016/j.chemosphere.2008.12.006.

3. Segura, P. A., Takada, H., Correa, J. A., El Saadi, K., Koike, T., Onwona-Agyeman, S., et al. (2015). Global occurrence of anti-infectives in contaminated surface waters: Impact of income inequality between countries. *Environment International, 80,* 89–97. https://doi.org/10.1016/j.envint.2015.04.001.

4. Carvalho, I. T., & Santos, L. (2016). Antibiotics in the aquatic environments: A review of the european scenario. *Environment International, 94,* 736–757. https://doi.org/10.1016/j.envint.2016.06.025.

5. Danner, M.-C., Robertson, A., Behrends, V., & Reiss, J. (2019). Antibiotic pollution in surface fresh waters: Occurrence and effects. *Science of the Total Environment, 664,* 793–804. https://doi.org/10.1016/j.scitotenv.2019.01.406.

6. O'Flynn, D., Lawler, J., Yusuf, A., Parle-McDermott, A., Harold, D., Mc Cloughlin, T., et al. (2021). A review of pharmaceutical occurrence and pathways in the aquatic environment in the context of a changing climate and the COVID-19 pandemic. *Analytical Methods, 13,* 575–594. https://doi.org/10.1039/D0AY02098B.

7. . Wilkinson, J.L., Boxall, A.B.A., Kolpin, D.W., Leung, K.M.Y., Lai, R.W.S., Galbán-Malagón, C., Adell, A.D., Mondon, J., Metian, M., Marchant, R.A., Bouzas-Monroy, A., Cuni-Sanchez, A., Coors, A., Carriquiriborde, P., Rojo, M., Gordon, C., Cara, M., Moermond, M., Luarte, T., Petrosyan, V., Perikhanyan, Y., Mahon, C.S., McGurk, C.J., Hofmann, T., Kormoker, T., Iniguez, V., Guzman-Otazo, J., Tavares, J.L., Gildasio De Figueiredo, F., Razzolini, M.T.P., Dougnon, V., Gbaguidi, G., Traoré, O., Blais, J.M., Kimpe, L.E., Wong, M., Wong, D., Ntchantcho, R., Pizarro, J., Ying, G.-G., Chen, C.-E., Páez, M., Martínez-Lara, J., Otamonga, J.-P., Poté, J., Ifo, S.A., Wilson, P., Echeverría-Sáenz, S., Udikovic-Kolic, N., Milakovic, M., Fatta-Kassinos, D., Ioannou-Ttofa, L., Belušová, V., Vymazal, J., Cárdenas-Bustamante, M., Kassa, B.A., Garric, J., Chaumot, A., Gibba, P., Kunchulia, I., Seidensticker, S., Lyberatos, G., Halldórsson, H.P., Melling, M., Shashidhar, T., Lamba, M., Nastiti, A., Supriatin, A., Pourang, N., Abedini, A., Abdullah, O., Gharbia, S.S., Pilla, F., Chefetz, B., Topaz, T., Yao, K.M., Aubakirova, B., Beisenova, R., Olaka, L., Mulu, J.K., Chatanga, P., Ntuli, V., Blama, N.T., Sherif, S., Aris, A.Z., Looi, L.J., Niang, M., Traore, S.T., Oldenkamp, R., Ogunbanwo, O., Ashfaq, M., Iqbal, M., Abdeen, Z., O'Dea, A., Morales-Saldaña, J.M., Custodio, M., de la Cruz, H., Navarrete, I., Carvalho, F., Gogra, A.B., Koroma, B.M., Cerkvenik-Flajs, V., Gombač, M., Thwala, M., Choi, K., Kang, H., Ladu, J.L.C., Rico, A., Amerasinghe, P., Sobek, A., Horlitz, G., Zenker, A.K., King, A.C., Jiang, J.-J., Kariuki, R., Tumbo, M., Tezel, U., Onay, T.T., Lejju, J.B., Vystavna, Y., Vergeles, Y., Heinzen, H., Pérez-Parada, A., Sims, D.B., Figy, M., Good, D., & Teta, C. (2022). Pharmaceutical pollution of the world's rivers. *Proceedings of the National Academy of Sciences of the United States of America, 119,* 2113947119. https://doi.org/10.1073/pnas.2113947119.

8. Loos, R., Gawlik, B. M., Locoro, G., Rimaviciute, E., Contini, S., & Bidoglio, G. (2008). EU Wide Monitoring Survey of Polar Persistent Pollutants in European River Waters. Publications Office, Gemeinsame Forschungsstelle and Institut für Umwelt und Nachhaltigkeit, Luxembourg. https://doi.org/10.2788/29668

9. Johnson, A. C., Keller, V., Dumont, E., & Sumpter, J. P. (2015). Assessing the concentrations and risks of toxicity from the antibiotics ciprofloxacin, sulfamethoxazole, trimethoprim and erythromycin in European rivers. *Science of the Total Environment, 511,* 747–755. https://doi.org/10.1016/j.scitotenv.2014.12.055.

10. Thiebault, T. (2020). Sulfamethoxazole/trimethoprim ratio as a new marker in raw wastewaters: A critical review. *Science of the Total Environment, 715,* 136916. https://doi.org/10.1016/j.scitotenv.2020.136916.

11. Zhou, W., & Moore, D. E. (1994). Photochemical decomposition of sulfamethoxazole. *International Journal of Pharmaceutics, 110,* 55–63. https://doi.org/10.1016/0378-5173(94)90375-1.

12. Moore, D. E., & Zhou, W. (1994). Photodegradation of sulfamethoxazole: A chemical system capable of monitoring seasonal changes in UVB intensity. *Photochemistry and Photobiology, 59,* 497–502. https://doi.org/10.1111/j.1751-1097.1994.tb02974.x.

13. Andreozzi, R., Raffaele, M., & Nicklas, P. (2003). Pharmaceuticals in STP effluents and their solar photodegradation in aquatic environment. *Chemosphere, 50,* 1319–1330. https://doi.org/10.1016/S0045-6535(02)00769-5.

14. Boreen, A. L., Arnold, W. A., & McNeill, K. (2004). Photochemical fate of sulfa drugs in the aquatic environment: Sulfa drugs containing five-membered heterocyclic groups. *Environmental Science and Technology, 38*(14), 3933–3940. https://doi.org/10.1021/es0353053.

15. Lam, M. W., & Mabury, S. A. (2005). Photodegradation of the pharmaceuticals atorvastatin, carbamazepine, levofloxacin, and sulfamethoxazole in natural waters. *Aqua Science, 67,* 177–188. https://doi.org/10.1007/s00027-004-0768-8.

16. Sona, M., Baus, C., & Brauch, H.-J. (2006). UV Irradiation versus combined UV/hydrogen peroxide and UV/ozone treatment for the removal of persistent organic pollutants from water. In: Wasser Berlin—International Conference Ozone and UV, April 3rd 2006, pp. 69–76.

17. Bayarri, B., Abellan, M. N., Gimenez, J., & Esplugas, S. (2007). Study of the wavelength effect in the photolysis and heterogeneous photocatalysis. *Catalysis Today, 129,* 231–239. https://doi.org/10.1016/j.cattod.2007.08.006.

18. Canonica, S., Meunier, L., & von Gunten, U. (2008). Phototransformation of selected pharmaceuticals during UV treatment of drinking water. *Water Research, 42,* 121–128. https://doi.org/10.1016/j.watres.2007.07.026.

19. Beltran, F. J., Aguinaco, A., & Garcia-Araya, J. F. (2009). Mechanism and kinetics of sulfamethoxazole photocatalytic ozonation in water. *Water Research, 43*(5), 1359–1369. https://doi.org/10.1016/j.watres.2008.12.015.

20. Baeza, C., & Knappe, D. R. U. (2011). Transformation kinetics of biochemically active compounds in low-pressure UV photolysis and UV/H_2O_2 advanced oxidation processes. *Water Research, 45*(15), 4531–4543. https://doi.org/10.1016/j.watres.2011.05.039.

21. Bonvin, F., Omlin, J., Rutler, R., Schweizer, W. B., Alaimo, P. J., Strathmann, T. J., et al. (2013). Direct photolysis of human metabolites of the antibiotic sulfamethoxazole: Evidence for abiotic back-transformation. *Environmental Science and Technology, 47*(13), 6746–6755. https://doi.org/10.1021/es303777k.

22. Batchu, S. R., Panditi, V. R., O'Shea, K. E., & Gardinali, P. R. (2014). Photodegradation of antibiotics under simulated solar radiation: Implications for their environmental fate. *Science of the Total Environment, 470–471,* 299–310. https://doi.org/10.1016/j.scitotenv.2013.09.057.

23. Długosz, M., Żmudzki, P., Kwiecień, A., Szczubiałka, K., Krzek, J., & Nowakowska, M. (2015). Photocatalytic degradation of sulfamethoxazole in aqueous solution using a floating TiO$_2$-expanded perlite photocatalyst. *Journal of Hazardous Materials, 298,* 146–153. https://doi.org/10.1016/j.jhazmat.2015.05.016.

24. Lian, J., Qiang, Z., Li, M., Bolton, J. R., & Qu, J. (2015). UV photolysis kinetics of sulfonamides in aqueous solution based on optimized fluence quantification. *Water Research, 75,* 43–50. https://doi.org/10.1016/j.watres.2015.02.026.

25. Ao, X., & Liu, W. (2017). Degradation of sulfamethoxazole by medium pressure UV and oxidants: Peroxymonosulfate, persulfate, and hydrogen peroxide. *Chemical Engineering Journal, 313,* 629–637. https://doi.org/10.1016/j.cej.2016.12.089.

26. Luo, S., Wei, Z., Spinney, R., Zhang, Z., Dionysiou, D. D., Gao, L., et al. (2018). UV direct photolysis of sulfamethoxazole and ibuprofen: An experimental and modelling study. *Journal of Hazardous Materials, 343,* 132–139. https://doi.org/10.1016/j.jhazmat.2017.09.019.

27. Wei, C., Li, X., Xie, Y., & Wang, X. (2019). Direct photo transformation of tetracycline and sulfanomide group antibiotics in surface water: Kinetics, toxicity and site modeling. *Science of the Total Environment, 686,* 1–9. https://doi.org/10.1016/j.scitotenv.2019.04.041.

28. Oliveira, C., Lima, D. L. D., Silva, C. P., Calisto, V., Otero, M., & Esteves, V. I. (2019). Photodegradation of sulfamethoxazole in environmental samples: The role of pH, organic matter and

salinity. *Science of the Total Environment, 648,* 1403–1410. https://doi.org/10.1016/j.scitotenv.2018.08.235.

29. Yu, H.-W., Park, M., Wu, S., Lopez, I. J., Ji, W., Scheideler, J., & Snyder, S. A. (2019). Strategies for selecting indicator compounds to assess attenuation of emerging contaminants during UV advanced oxidation processes. *Water Research, 166,* 115030. https://doi.org/10.1016/j.watres.2019.115030.

30. Lastre-Acosta, A. M., Cristofoli, B. S., Parizi, M. P. S., Oller do Nascimento, C. A., & Teixeira, A. C. S. C. (2021). Photochemical persistence of sulfa drugs in aqueous medium: Kinetic study and mathematical simulations. *Environmental Science and Pollution Research, 28,* 23887–23895. https://doi.org/10.1007/s11356-020-11715-x.

31. Borowska, E., Felis, E., & Miksch, K. (2015). Degradation of sulfamethoxazole using UV and UV/H_2O_2 processes. *Journal of Advanced Oxidation Technologies, 18,* 69–77. https://doi.org/10.1515/jaots-2015-0109.

32. Carlson, J. C., Stefan, M. I., Parnis, J. M., & Metcalfe, C. D. (2015). Direct UV photolysis of selected pharmaceuticals, personal care products and endocrine disruptors in aqueous solution. *Water Research, 84,* 350–361. https://doi.org/10.1016/j.watres.2015.04.013.

33. Yang, Y., Lu, X., Jiang, J., Ma, J., Liu, G., Cao, Y., et al. (2017). Degradation of sulfamethoxazole by UV, UV/H_2O_2 and UV/persulfate (PDS): Formation of oxidation products and effect of bicarbonate. *Water Research, 118,* 196–207. https://doi.org/10.1016/j.watres.2017.03.054.

34. Kwon, M., Yoon, Y., Kim, S., Jung, Y., Hwang, T. M., & Kang, J.-W. (2018). Removal of sulfamethoxazole, ibuprofen and nitrobenzene by UV and UV/chlorine processes: A comparative evaluation of 275 nm LED-UV and 254 nm LP-UV. *Science of the Total Environment, 637–638,* 1351–1357. https://doi.org/10.1016/j.scitotenv.2018.05.080.

35. Chowdhury, P., Sarathy, S. R., Das, S., Li, J., Ray, A. K., & Ray, M. B. (2020). Direct UV photolysis of pharmaceutical compounds: Determination of pH-dependent quantum yield and full-scale performance. *Chemical Engineering Journal, 380,* 122460. https://doi.org/10.1016/j.cej.2019.122460.

36. Rodriguez-Blanco, L. A. J., Ocampo-Pérez, R., Gómez-Durán, C. F. A., Mojica-Sánchez, J. P., & Razo-Hernández, R. S. (2020). Removal of sulfamethoxazole, sulfadiazine, and sulfamethazine by UV radiation and HO· and SO$_4$·⁻ radicals using a response surface model and DFT calculations. *Environmental Science and Pollution Research, 27,* 41609–41622. https://doi.org/10.1007/s11356-020-10071-0.

37. Zhang, R., Yang, Y., Huang, C.-H., Li, N., Liu, H., Zhao, L., & Sun, P. (2016). UV/H_2O_2 and UV/PDS treatment of trimethoprim and sulfamethoxazole in synthetic human urine: Transformation products and toxicity. *Environmental Science and Technology, 50,* 2573–2583. https://doi.org/10.1021/acs.est.5b05604.

38. Alharbi, S. K., Kang, J., Nghiem, L. D., van de Merwe, J. P., Leusch, F. D. L., & Price, W. E. (2017). Photolysis and UV/H_2O_2 of diclofenac, sulfamethoxazole, carbamazepine, and trimethoprim: Identification of their major degradation products by ESI-LC–MS and assessment of the toxicity of reaction mixtures. *Process Safety and Environmental Protection, 112,* 222–234. https://doi.org/10.1016/j.psep.2017.07.015.

39. Huber, M. M., Canonica, S., Park, G.-Y., & von Gunten, U. (2003). Oxidation of pharmaceuticals during ozonation and advanced oxidation processes. *Environmental Science and Technology, 37*(5), 1016–1024. https://doi.org/10.1021/es025896h.

40. Dantas, R. F., Contreras, S., Sans, C., & Esplugas, S. (2008). Sulfamethoxazole abatement by means of ozonation. *Journal of Hazardous Materials, 150,* 790–794. https://doi.org/10.1016/j.jhazmat.2007.05.034.

41. Lee, Y., Gerrity, D., Lee, M., Bogeat, A. E., Salhi, E., Gamage, S., et al. (2013). Prediction of micropollutant elimination during ozonation of municipal wastewater effluents: Use of kinetic and water specific information. *Environmental Science and Technology, 47,* 5872–5881. https://doi.org/10.1021/es400781r.

42. Wu, W., Bai, L., Song, Y., Su, Y., Jiang, K., Sun, H., et al. (2021). Defect-engineered graphene films as ozonation catalysts for the devastation of sulfamethoxazole: Insights into the active sites and oxidation mechanism. *ACS Applied Materials and Interfaces, 13,* 52706–52716. https://doi.org/10.1021/acsami.1c16920.

43. Ben, W., Shi, Y., Li, W., Zhang, Y., & Qiang, Z. (2017). Oxidation of sulfonamide antibiotics by chlorine dioxide in water: Kinetics and reaction pathways. *Chemical Engineering Journal, 327,* 743–750. https://doi.org/10.1016/j.cej.2017.06.157.

44. Lee, Y., Gerrity, D., Lee, M., Gamage, S., Pisarenko, A., Trenholm, R. A., et al. (2016). Organic contaminant abatement in reclaimed water by UV/H_2O_2 and a combined process consisting of O_3/H_2O_2 followed by UV/H_2O_2: Prediction of abatement efficiency, energy consumption, and byproduct formation. *Environmental Science and Technology, 50*(7), 3809–3819. https://doi.org/10.1021/acs.est.5b04904.

45. Prasannamedha, G., & Kumar, P. S. (2020). A review on contamination and removal of sulfamethoxazole from aqueous solution using cleaner techniques: Present and future perspective. *Journal of Cleaner Production, 250,* 119553. https://doi.org/10.1016/j.jclepro.2019.119553.

46. Puhlmann, N., Olsson, O., & Kümmerer, K. (2022). Transformation products of sulfonamides in aquatic systems: Lessons learned from available environmental fate and behaviour data. *Science of the Total Environment, 830,* 154744. https://doi.org/10.1016/j.scitotenv.2022.154744.

47. Ullman, E. F., & Singh, B. (1966). Photochemical transposition of ring atoms in five-membered heterocycles, The photorearrangement of 3,5-diphenylisoxazole. *Journal of the American Chemical Society, 88,* 1844–1845. https://doi.org/10.1021/ja00960a066.

48. Palacios, F., de Retana, A. M. O., de Marigorta, E. M., & de los Santos, J. M. (2002). Preparation properties and synthetic applications of 2H-azirines: A review. *Organic Preparations and Procedures International, 34,* 219–269. https://doi.org/10.1080/00304940209356770.

49. Galenko, E. E., Khlebnikov, A. F., & Novikov, M. S. (2016). Isoxazole-azirine isomerization as a reactivity switch in the synthesis of heterocycles. *Chemistry of Heterocyclic Compounds, 52,* 637–650. https://doi.org/10.1007/s10593-016-1944-1.

50. Boulton, A. J., & Katritzky, A. R. (1961). The tautomerism of heteroaromatic compounds with five-membered rings—II: 3-,4- and 5-amino- and acetamido-isoxazoles. *Tetrahedron, 12,* 51–55. https://doi.org/10.1016/0040-4020(61)80098-7.

51. Lam, M. W., Young, C. J., Brain, R. A., Johnson, D. J., Hanson, M. A., Wilson, C. J., et al. (2004). Aquatic persistence of eight pharmaceuticals in a microcosm study. *Environmental Toxicology and Chemistry, 23,* 1431–1440. https://doi.org/10.1897/03-421.

52. Trovo, A. G., Nogueira, R. F. P., Agueera, A., Sirtori, C., & Fernandez-Alba, A. R. (2009). Photodegradation of sulfamethoxazole in various aqueous media: Persistence, toxicity and photoproducts assessment. *Chemosphere.* https://doi.org/10.1016/j.chemosphere.2009.09.065.

53. Poirier-Larabie, S., Segura, P. A., & Gagnona, C. (2016). Degradation of the pharmaceuticals diclofenac and sulfamethoxazole and their transformation products under controlled environmental conditions. *Science of the Total Environment, 557–558,* 257–267. https://doi.org/10.1016/j.scitotenv.2016.03.057.

54. Willach, S., Lutze, H. V., Eckey, K., Löppenberg, K., Lüling, M., Wolbert, J.-B., et al. (2018). Direct photolysis of sulfamethoxazole using various irradiation sources and wavelength ranges—Insights from degradation product analysis and compound-specific stable

isotope analysis. *Environmental Science and Technology, 52,* 1225–1233. https://doi.org/10.1021/acs.est.7b04744.

55. Su, T., Deng, H., Benskin, J. P., & Radke, M. (2016). Biodegradation of sulfamethoxazole photo-transformation products in a water/sediment test. *Chemosphere, 148,* 518–525. https://doi.org/10.1016/j.chemosphere.2016.01.049.

56. Baena-Nogueras, R. M., González-Mazo, E., & Lara-Martín, P. A. (2017). Photolysis of antibiotics under simulated sunlight irradiation: Identification of photoproducts by high-resolution mass spectrometry. *Environmental Science and Technology, 51,* 3148–3156. https://doi.org/10.1021/acs.est.6b03038.

57. Niu, J., Zhang, L., Li, Y., Zhao, J., Lv, S., & Xiao, K. (2013). Effects of environmental factors on sulfamethoxazole photodegradation under simulated sunlight irradiation: Kinetics and mechanism. *Journal of Environmental Science, 25,* 1098–1106. https://doi.org/10.1016/S1001-0742(12)60167-3.

58. Palm, W.-U. (2018). Photochemistry of 9-acridinecarboxaldehyde in aqueous media. *Photochemical and Photobiological Sciences, 17,* 964–974. https://doi.org/10.1039/C8PP00185E.

59. Palm, W.-U. (2017). Oxygen dependence in the photoreaction of the pesticide metamitron. *Journal of Photochemistry and Photobiology, 347,* 138–145. https://doi.org/10.1016/S1010-6030(02)00426-4.

60. Braslavsky, S. E. (2007). Glossary of terms used in photochemistry, 3rd edition (IUPAC recommendations 2006). *Pure and Applied Chemistry, 79,* 293–465. https://doi.org/10.1351/pac200779030293.

61. Löher, F., Palm, W.-U., Schaffer, M., & Olsson, O. (2021). Concentrations and sources of methylxanthines in a northern German river system. *Science of the Total Environment, 775,* 145898. https://doi.org/10.1016/j.scitotenv.2021.145898.

62. Sherrod, P. H. (2013). Nonlinear regression and curve fitting program NLREG, version 6.5 (advanced). 9207 Brushboro Drive, Brentwood, TN 37027, USA. 9207 Brushboro Drive.

63. Connors, K. A. (1990). *Chemical kinetics*. VCH.

64. Grimme, S., Bohle, F., Hansen, A., Pracht, P., Spicher, S., & Stahn, M. (2021). Efficient quantum chemical calculation of structure ensembles and free energies for nonrigid molecules. *The Journal of Physical Chemistry A, 125,* 4039–4054. https://doi.org/10.1021/acs.jpca.1c00971.

65. Spicher, S., & Grimme, S. (2020). Robust atomistic modeling of materials, organometallic, and biochemical systems. *Angewandte Chemie International Edition, 59,* 15665–15673. https://doi.org/10.1002/anie.202004239.

66. Grimme, S., Bannwarth, C., & Shushkov, P. (2017). A robust and accurate tight-binding quantum chemical method for structures, vibrational frequencies, and noncovalent interactions of large molecular systems parametrized for all SPD-block elements ($z = 1$–86). *Journal of Chemical Theory and Computation, 13,* 1989–2009. https://doi.org/10.1021/acs.jctc.7b00118.

67. Pracht, P., Bohle, F., & Grimme, S. (2020). Automated exploration of the low-energy chemical space with fast quantum chemical methods. *Physical Chemistry Chemical Physics, 22,* 7169–7192. https://doi.org/10.1039/C9CP06869D.

68. Grimme, S., Hansen, A., Ehlert, S., & Mewes, J.-M. (2021). r^2 scan-3c: A swiss army knife composite electronic-structure method. *The Journal of Chemical Physics, 154,* 064103. https://doi.org/10.1063/5.0040021.

69. Ehlert, S., Stahn, M., Spicher, S., & Grimme, S. (2021). Robust and efficient implicit solvation model for fast semiempirical methods. *Journal of Chemical Theory and Computation, 17,* 4250–4261. https://doi.org/10.1021/acs.jctc.1c00471.

70. Klamt, A. (1995). Conductor-like screening model for real solvents: A new approach to the quantitative calculation of solvation phenomena. *The Journal of Physical Chemistry A, 99,* 2224–2235. https://doi.org/10.1021/j100007a062.

71. Klamt, A., Jonas, V., Bürger, T., & Lohrenz, J. C. W. (1998). Refinement and parametrization of Cosmo-RS. *The Journal of Physical Chemistry A, 102,* 5074–5085. https://doi.org/10.1021/jp980017s.

72. Pracht, P., & Grimme, S. (2021). Efficient quantum-chemical calculations of acid dissociation constants from free-energy relationships. *The Journal of Physical Chemistry A, 125,* 5681–5692. https://doi.org/10.1021/acs.jpca.1c03463.

73. Gmurek, M., Horn, H., & Majewsky, M. (2015). Phototransformation of sulfamethoxazole under simulated sunlight: Transformation products and their antibacterial activity toward vibrio fischeri. *Science of the Total Environment, 538,* 58–63. https://doi.org/10.1016/j.scitotenv.2015.08.014.

74. Vree, T. B., van der Ven, A. J. A. M., Verwey-van Wissen, C. P. W. G. M., van Ewijk-Beneken Kolmer, E. W. J., Swolfs, A. E. M., van Galen, P. M., & Amatdjais-Groenen, H. (1994). Isolation, identification and determination of sulfamethoxazole and its known metabolites in human plasma and urine by high-performance liquid chromatography. *Journal of Chromatography B: Biomedical Sciences and Applications, 658,* 327–340. https://doi.org/10.1016/0378-4347(94)00232-0.

75. Majewsky, M., Wagner, D., Delay, M., Bräse, S., Yargeau, V., & Horn, H. (2014). Antibacterial activity of sulfamethoxazole transformation products (TPS): General relevance for sulfonamide TPS modified at the para position. *Chemical Research in Toxicology, 27,* 1821–1828. https://doi.org/10.1021/tx500267x.

76. Majewsky, M., Glauner, T., & Horn, H. (2015). Systematic suspect screening and identification of sulfonamide antibiotic transformation products in the aquatic environment. *Analytical and Bioanalytical Chemistry, 407,* 5707–5717. https://doi.org/10.1007/s00216-015-8748-5.

77. Scholes, R. C., Prasse, C., & Sedlak, D. L. (2019). The role of reactive nitrogen species in sensitized photolysis of wastewater-derived trace organic contaminants. *Environmental Science and Technology, 53,* 6483–6491. https://doi.org/10.1021/acs.est.9b01386.

78. Zhang, Y., Li, L., Pan, Z., Zhu, Y., Shao, Y., Wang, Y., & Yu, K. (2020). Degradation of sulfamethoxazole by UV/persulfate in different water samples: Influential factors, transformation products and toxicity. *Chemical Engineering Journal, 379,* 122354. https://doi.org/10.1016/j.cej.2019.122354.

79. Hu, L., Flanders, P. M., Miller, P. L., & Strathmann, T. J. (2007). Oxidation of sulfamethoxazole and related antimicrobial agents by TiO$_2$ photocatalysis. *Water Research, 41,* 2612–2626. https://doi.org/10.1016/j.watres.2007.02.026.

80. Periša, M., Babić, S., Škorić, I., Frömel, T., & Knepper, T. P. (2013). Photodegradation of sulfonamides and their 4-acetylated metabolites in water by simulated sunlight irradiation: Kinetics and identification of photoproducts. *Environmental Science and Pollution Research, 12,* 8934–8946. https://doi.org/10.1007/s11356-013-1836-1.

81. Qiang, Z., & Adams, C. (2004). Potentiometric determination of acid dissociation constants (p*K*a) for human and veterinary antibiotics. *Water Research, 38*(12), 2874–2890. https://doi.org/10.1016/j.watres.2004.03.017.

82. Lin, C.-E., Lin, W.-C., Chen, Y.-C., & Wang, S.-W. (1997). Migration behavior and selectivity of sulfonamides in capillary electrophoresis. *Journal of Chromatography A, 792*(1), 37–47. https://doi.org/10.1016/S0021-9673(97)00614-6.

83. Ge, L., Zhang, P., Halsall, C., Li, Y., Chen, C.-E., Li, J., et al. (2019). The importance of reactive oxygen species on the aqueous phototransformation of sulfonamide antibiotics: Kinetics, pathways, and comparisons with direct photolysis. *Water Research, 149,* 243–250. https://doi.org/10.1016/j.watres.2018.11.009.

84. Geiser, L., Henchoz, Y., Galland, A., Carrupt, P.-A., & Veuthey, J.-L. (2005). Determination of pka values by capillary zone

electrophoresis with a dynamic coating procedure. *Journal of Separation Science, 28,* 2374–2380. https://doi.org/10.1002/jssc.200500213.

85. Kortüm, G., Andrussow, K., & Vogel, W. (1961). Dissoziationskonstanten Organischer Säuren in Wässriger Lösung (International Union of Pure and Applied Chemistry. Section of Analytical Chemistry Commission on Electrochemical Data). Butterworths, London.

86. Dahlan, R., Mcdonald, C., & Sunderland, V. B. (1987). Solubilities and intrinsic dissolution rates of sulphamethoxazole and trimethoprim. *Journal of Pharmacy and Pharmacology, 39,* 246–251. https://doi.org/10.1111/j.2042-7158.1987.tb06261.x.

87. Martínez, F., & Gómez, A. (2001). Thermodynamic study of the solubility of some sulfonamides in octanol, water, and the mutually saturated solvents. *Journal of Solution Chemistry, 30,* 909–923. https://doi.org/10.1023/A:1012723731104.

88. Kratochwil, N. A., Huber, W., Müller, F., Kansy, M., & Gerber, P. R. (2002). Predicting plasma protein binding of drugs: A new approach. *Biochem Pharmaceuticals, 64*(9), 1355–1374. https://doi.org/10.1016/S0006-2952(02)01074-2.

89. Szczepaniak, W., & Szymanski, A. (2000). Relationship between hydrophobic properties of amphoteric sulfonamides and their retention in micellar reversed phase liquid chromatography. *Journal of Liquid Chromatography and Related Technologies, 23,* 1217–1231. https://doi.org/10.1081/JLC-100100410.

90. Leo, A., Hansch, C., & Elkins, D. (1971). Partition coefficients and their uses. *Chemical Reviews, 71,* 525–616. https://doi.org/10.1021/cr60274a001.

91. Salthammer, T., Grimme, S., Stahn, M., Hohm, U., & Palm, W.-U. (2022). Quantum chemical calculation and evaluation of partition coefficients for classical and emerging environmentally relevant organic compounds. *Environmental Science and Technology, 56*(1), 379–391. https://doi.org/10.1021/acs.est.1c06935.

92. EPA: EPI-SUITE, Version 4.11. (2012). Environmental Protection Agency, Washington (2012).

93. Ruggaber, A., Dlugi, R., & Nakajima, T. (1994). Modelling radiation quantities and photolysis frequencies in the troposphere. *Journal of Atmospheric Chemistry, 18,* 171–210. https://doi.org/10.1007/BF00696813.

94. Mohatt, J. L., Hu, L., Finneran, K. T., & Strathmann, T. J. (2011). Microbially mediated abiotic transformation of the antimicrobial agent sulfamethoxazole under iron-reducing soil conditions. *Environmental Science and Technology, 45,* 4793–4801. https://doi.org/10.1021/es200413g.

95. Wang, Y., Zhang, H., Li, B., Yu, M., Zhao, R., Xu, X., & Cai, L. (2019). γ-FeOOH graphene polyacrylamide carbonized aerogel as air-cathode in electro-Fenton process for enhanced degradation of sulfamethoxazole. *Chemical Engineering Journal, 359,* 914–923. https://doi.org/10.1016/j.cej.2018.11.096.

96. Birks, J. B. (1973). Organic molecular photophysics. Wiley monographs in chemical physics, vol. 1. Wiley.

97. Turro, N. J., Ramamurthy, V., Cherry, W., & Farneth, W. (1978). The effect of wavelength on organic photoreactions in solution. Reactions from upper excited states. *Chemical Reviews, 78,* 125–145. https://doi.org/10.1021/cr60312a003.

98. Bahnmüller, S., von Gunten, U., & Canonica, S. (2014). Sunlight-induced transformation of sulfadiazine and sulfamethoxazole in surface waters and wastewater effluents. *Water Research, 57,* 183–192. https://doi.org/10.1016/j.watres.2014.03.019.

Authors and Affiliations

Wolf-Ulrich Palm[1] 🆔 **· Nicola Schmidt[1] · Marcel Stahn[2] · Stefan Grimme[2]**

Nicola Schmidt
schmidt-nicola@gmx.de

Marcel Stahn
stahn@thch.uni-bonn.de

Stefan Grimme
grimme@thch.uni-bonn.de

[1] Institute for Sustainable Chemistry, Leuphana University, Universitätsallee 1, 21335 Lüneburg, Germany

[2] Mulliken Center for Theoretical Chemistry, University of Bonn, Beringstraße 4, 53115 Bonn, Germany